Inorg. Chem. **2005**, *44*, 197–205

Structural Chemistry of A_3CuBO_6 (A = Ca, Sr; B = Mn, Ru, Ir) as a Function of Temperature

A. Sam Aldridge,[†] Peter D. Battle,*[,†] John S. O. Evans,[‡] Caroline A. Moore,[†] Timothy J. Prior,[†] and Philip J. Wiseman[†]

Inorganic Chemistry Laboratory, Oxford University, South Parks Road, Oxford OX1 3QR, U.K., and Department of Chemistry, University Science Laboratories, South Road, Durham DH1 3LE, U.K.

Received September 3, 2004

Variable temperature X-ray and neutron powder diffraction techniques have been used to identify structural phase transitions in Cu-rich $A_3A'BO_6$ phases. A transition from monoclinic to rhombohedral symmetry was observed by X-ray diffraction between 700 and 500 K in $Sr_3Cu_{1-x}M_xIrO_6$ (M = Ni, Zn; $0 \leq x \leq 0.5$). The temperature of the phase change decreased in a linear manner with Cu-content and was essentially independent of the nature of M. $Ca_{3.1}Cu_{0.9}MnO_6$ was shown to pass from a rhombohedral phase to a triclinic phase on cooling below 290 K; the structure of the triclinic phase was refined against neutron diffraction data collected at 2 K. $Ca_{3.1}Cu_{0.9}RuO_6$ undergoes a transition between a disordered rhombohedral phase and an ordered monoclinic phase when cooled below 623 K. Neutron diffraction has been used to determine the structure as a function of temperature in the range $523 \leq T/K \leq 723$ and hence to determine an order parameter for the low temperature phase; the second-order transition is shown to be incomplete 100 K below the critical temperature.

Introduction

The resurgence of interest in the long-established K_4CdCl_6 structure[1] has been fueled by the wide variety of oxide analogues that can be prepared, for example Sr_4PtO_6,[2] $Sr_3A'IrO_6$ (A′ = Ni, Cu, Zn),[3] $Sr_3A'NiO_6$ (A′ = Sc, In, Tm, Yb, Lu),[4] Sr_3MgBO_6 (B = Pt, Ir, Rh),[5] Sr_3ZnPtO_6,[6] and $Ca_3A'MnO_6$ (A′ = Ni, Zn).[7] The structures of these $A_3A'BO_6$ materials consist of polyhedral chains made up from alternating $A'O_6$ trigonal prisms and BO_6 octahedra, the A sites in the interchain space usually being occupied by Ca^{2+} or Sr^{2+} cations. While the majority of these phases retain the rhombohedral crystal symmetry of the parent compound, it has been found that introduction of Cu^{2+} onto the prismatic site results in subtle changes to the crystal structure. Thus, while the structures of Sr_3CuPtO_6[8] and Sr_3CuIrO_6[9] are broadly similar to that of K_4CdCl_6, there is an important difference in that the Cu^{2+} cation is displaced from the center of the prism toward a rectangular face so as to lower the electronic energy of the Jahn−Teller active d^9 cation. This displacement occurs in an ordered manner and therefore has the consequence of lowering the symmetry of these phases to monoclinic (Figure 1). All but one of the of Cu-containing $A_3A'BO_6$ phases known at the time this study commenced adopt this modification of the K_4CdCl_6 structure in space group $C2/c$, the exception being $Ca_{3.5}Cu_{0.5}PtO_6$[10] which has been shown by single-crystal X-ray diffraction to crystallize in the space group $C2$. In this composition, the prisms are occupied alternately by Cu^{2+} and Ca^{2+}. More recently, Zubkov et al.[11] have reported a study on a polycrystalline sample of composition Ca_3CuMnO_6 in which they found it necessary to reduce the crystal symmetry further to triclinic ($P\bar{1}$) in order to account for all the observed diffraction peaks. The triclinic unit cell is closely related to that of the

* To whom correspondence should be addressed. E-mail: peter.battle@chem.ox.ac.uk.
[†] Oxford University.
[‡] University Science Laboratories, Durham.

(1) Bergerhoff, G.; Schmitz-Dumont, O. *Z. Anorg. Allg. Chem.* **1956**, *284*, 10−14.
(2) Randall, J. J.; Katz, L. *Acta Crystallogr.* **1959**, *12*, 519−521.
(3) Nguyen, T. N.; zur Loye, H.-C. *J. Solid State Chem.* **1995**, *117*, 300−308.
(4) James, M.; Attfield, J. P. *Chem.—Eur. J.* **1996**, *2*, 737−741.
(5) Nunez, P.; Trail, S.; zur Loye, H.-C. *J. Solid State Chem.* **1997**, *130*, 35−41.
(6) Lampe Onnerud, C.; zur Loye, H.-C. *Inorg. Chem.* **1996**, *35*, 2155−2156.
(7) Kawasaki, S.; Takano, M.; Inami, T. *J. Solid State Chem.* **1999**, *145*, 302−308.
(8) Wilkinson, A. P.; Cheetham, A. K.; Kunnman, W.; Kvick, A. *Eur. J. Solid State Inorg. Chem.* **1991**, *28*, 453−459.
(9) Neubacher, M.; Müller-Buschbaum, H. *Z. Anorg. Allg. Chem.* **1992**, *607*, 124−127.
(10) Tomaszewska, A.; Müller-Buschbaum, H. *Z. Anorg. Allg. Chem.* **1992**, *617*, 23−26.

10.1021/ic0487629 CCC: $30.25
Published on Web 12/21/2004

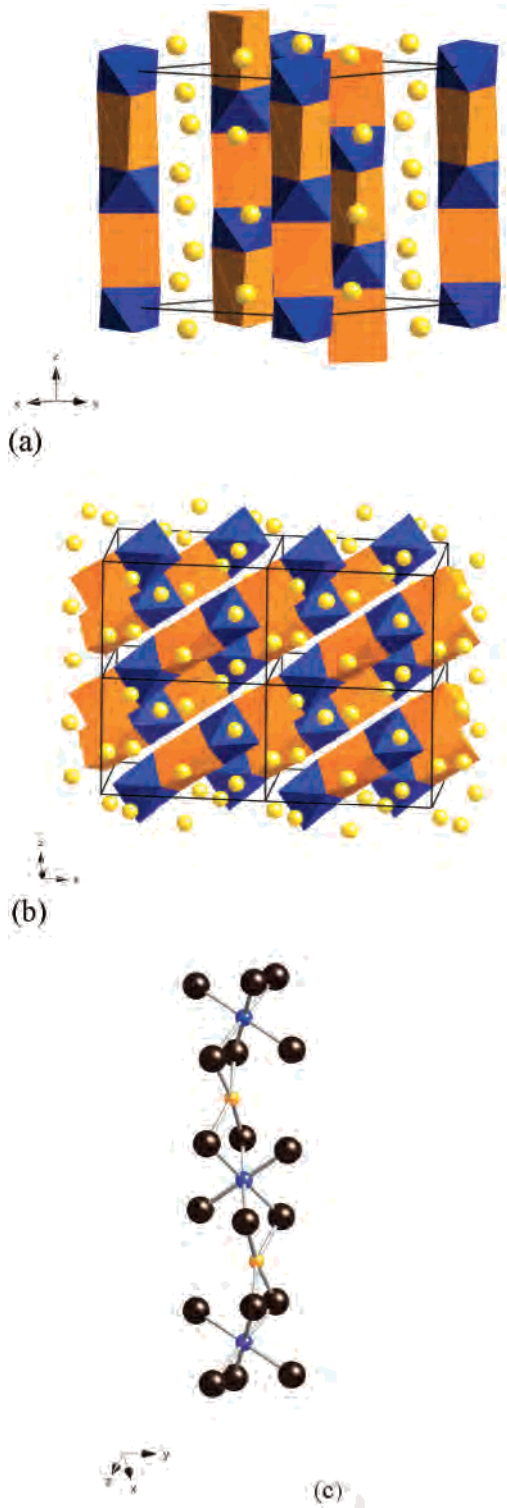

Figure 1. Unit cell of (a) Sr_4PtO_6, space group $R\bar{3}c$, and (b) Sr_3CuPtO_6, space group $C2/c$; circles represent Sr, light and dark shaded polyhedra are prisms and octahedra, respectively. (c) Atomic arrangement within a [101] polyhedral chain of monoclinic Sr_3CuPtO_6. Black circles represent O, light and dark small circles Cu and Pt, respectively.

monoclinic Sr_3CuPtO_6 phase, with the reduction in symmetry being attributed to a subtly different ordering of the Cu displacement vectors.

As described above, the departure from rhombohedral symmetry in these materials is ascribed to the Jahn−Teller activity of the Cu^{2+} cation. Niazi et al.[12] have studied the solid solution $Sr_3Cu_{1-x}Zn_xIrO_6$ and shown that the monoclinic distortion cannot be detected at room temperature for $x \geq 0.5$. In addition to being dependent on the concentration of Cu^{2+}, it is likely that the symmetry of these compounds changes with temperature. In this paper, we describe an exploration of the evolution with temperature of the crystal structure of selected Cu^{2+}-containing $A_3A'BO_6$ phases by appropriate combinations of differential scanning calorimetry (DSC), X-ray powder diffraction, and neutron powder diffraction.

Experimental Section

Polycrystalline samples of a number of target phases were synthesized using the standard methods of solid state chemistry. Compositions in the solid solutions $Sr_3Cu_{1-x}M_xIrO_6$ (M = Ni, Zn; $0 \leq x \leq 0.5$) were prepared by firing appropriate stoichiometric mixtures of $SrCO_3$, CuO, NiO, ZnO, and Ir at 800 °C for 24 h and then at 1150 °C in pellet form for 5 days. $Ca_{3.1}Cu_{0.9}MnO_6$ was prepared from stoichiometric quantities of $CaCO_3$, CuO, and MnO_2. The reagents were intimately ground and heated at 800 °C overnight and then, in pellet form, at 1000 °C for 18 days and 1100 °C for 9 days with frequent regrinding. $Ca_{3.1}Cu_{0.9}RuO_6$ was prepared as described previously.[13]

The progress of the reactions was followed using X-ray powder diffraction, and the reactions were deemed to be complete when there was no improvement in the quality of the diffraction pattern on further heating. Data suitable for Rietveld refinement were collected on each reaction product at room temperature (302 K) using a Cu $K\alpha_1$ Siemens D5000 diffractometer, operating over the angular range $10 \leq 2\theta/\text{deg} \leq 100$ with a step size of $\Delta 2\theta = 0.02°$. Data were collected on $Sr_3Cu_{1-x}M_xIrO_6$ above room temperature using a Siemens D5005 diffractometer fitted with a Goebel mirror and an Anton Paar HTK 1200 furnace, and operating with Cu Kα radiation. The temperature of the furnace was calibrated by inserting a Pt/10%Rh,Pt thermocouple through the X-ray window foil into the center of an empty sample cup, while using the instrumental thermocouple to stabilize the system. Phase changes were identified by following the reduction in the splitting of certain highly symmetry-dependent diffraction peaks, particularly those in the angular region $30 \leq 2\theta/\text{deg} \leq 45$, while collecting data over increasingly narrow temperature ranges using a temperature step size as small as 5 K. A data-collection time 2.5 h per temperature point was used. In this way, and with the resolution available, we believe we were able to identify the transition temperature to ±15 K. In the case of $Ca_{3.1}Cu_{0.9}MnO_6$, X-ray data were also collected on a Siemens D8 diffractometer while the sample was cooled at a rate of 6 K h^{-1} through the temperature range $300 > T/\text{K} > 16$; the data were summed hourly, to give a temperature resolution of 6 K.

Neutron powder diffraction experiments were carried out on $Ca_{3.1}Cu_{0.9}MnO_6$ at 293 and 2 K using the time-of-flight (TOF) instrument HRPD at the ISIS neutron source, Rutherford Appleton Laboratory, U.K. $Ca_{3.1}Cu_{0.9}RuO_6$ was studied over the temperature range $302 \leq T/\text{K} \leq 743$ using the constant-wavelength (CW) diffractometer D2b at ILL, Grenoble, France. The samples were contained in vanadium cans.

All diffraction data were analyzed using the GSAS program package. Peak shapes were modeled using either an exponential pseudo-

(11) Zubkov, V. G.; Bazuev, G. V.; Tyutyunnik, A. P.; Berger, I. F. *J. Solid State Chem.* **2001**, *160*, 293−301.
(12) Niazi, A.; Sampathkumaran, E. V.; Paulose, P. L.; Eckert, D.; Handstein, A.; Muller, K. H. *Phys. Rev. B* **2002**, *65*, 064418.
(13) Moore, C. A.; Cussen, E. J.; Battle, P. D. *J. Solid State Chem.* **2000**, *153*, 254−262.

Voigt convolution (ISIS TOF data) or a pseudo-Voigt function (CW data). The background level was modeled using a Chebyshev polynomial, except in the case of the neutron diffraction data from $Ca_{3.1}Cu_{0.9}RuO_6$ when a Fourier cosine summation was used. Regions of the diffraction patterns that were contaminated by scattering from the sample holder were omitted from the data analyses.

When appropriate, DSC data were collected on a Rheometric Scientific STA-1500 thermobalance, in an atmosphere of static air.

Results

(i) $Ca_{3.1}Cu_{0.9}MnO_6$. The original target of this synthesis was Ca_3CuMnO_6, but the X-ray diffraction pattern of the reaction product could be indexed in neither a Sr_3CuPtO_6-like monoclinic unit cell nor in a triclinic unit cell similar to that proposed by Zubkov et al. for the same composition, and it was therefore concluded that our sample was not monophasic. In light of our previous experiences with the Ca−Cu−Ru−O and Ca−Cu−Ir−O[3,14] systems, where we successfully prepared polycrystalline $Ca_{3.1}Cu_{0.9}RuO_6$ and $Ca_{3.1}Cu_{0.9}IrO_6$ after failing to prepare Ca_3CuRuO_6 and Ca_3CuIrO_6, we changed our target composition to $Ca_{3.1}Cu_{0.9}MnO_6$. Although the X-ray diffraction pattern collected from the new reaction product at 302 K showed the presence of 1.4(1)% by mass of CaO, the remaining peaks could all be accounted for using a rhombohedral Sr_4PtO_6-like unit cell. It proved impossible to eliminate this small impurity by varying the synthesis conditions. Close inspection of individual diffraction maxima established that the full width at half-maximum was ∼0.09° at $2\theta = 50°$, close to the resolution limit of the instrument. There was thus no evidence of a monoclinic or triclinic distortion. The structure was therefore refined in space group $R\bar{3}c$ with Cu and Ca occupying the 12*c* (0, 0, $^1/_4$) site in a 9:1 ratio. The refinement proceeded smoothly, although the atomic displacement parameter associated with the cations on the prismatic site took an unusually large value ($U_{iso} = 0.088(3)$ Å^2). A difference Fourier map suggested that these cations were displaced toward the rectangular faces of the prism in a disordered manner, and the Cu^{2+} and Ca^{2+} cations were therefore moved off the 3-fold axis to an 18*e* (*x*, 0, $^1/_4$) site with an occupancy factor of $^1/_3$; in view of the limited data set it was not possible to treat the Cu and Ca atoms separately. This strategy led to convergence of the least-squares analysis with $R_{wp} = 8.5\%$ and $\chi^2 = 1.1$, although the values of the displacement parameters remained relatively high. The refined values of the structural parameters are listed in Table 1, and the observed and calculated diffraction profiles are plotted in Figure 2.

Initial attempts to analyze the neutron diffraction data collected on the same sample at 293 K, taking the structure refined against the X-ray data as a starting point, were unsuccessful. It was apparent that supposedly single peaks at relatively high *d* spacings showed signs of a shoulder, as in Figure 3a. Attempts to model the data by lowering the symmetry to monoclinic or triclinic were unsuccessful. However, the fit to the data did improve when a two-phase model comprising a disordered rhombohedral phase and a triclinic phase, the latter based on the structure reported for Ca_3CuMnO_6, was used (Figure 4); no contribution from the CaO impurity could be detected in the neutron diffraction data. The refinement showed that 66.0(7)% of the sample was in the rhombohedral form, and 34.0(7)% in the triclinic form. In view of the large number of correlated variables involved in these refinements, the atomic displacement parameters were constrained to be zero. The neutron data collected at 2 K provided no evidence for the presence of two phases, and a single-phase refinement of a triclinic model proceeded smoothly; all attempts to increase the crystal symmetry failed. During these refinements, it was again necessary to constrain the values of the atomic displacement parameters to be zero. Attempts were made to refine the Ca/Cu ratio on the prismatic site, but no significant deviation from the ideal 10% value was found. Given the contrast between the negative scattering length of Mn and the positive values of Cu and Ca, we can be confident that only Mn is present on the octahedral sites. The fitted diffraction profile is drawn in Figure 5, and the lattice parameters, structural parameters and bond lengths are listed in Tables 2−4, respectively. The atomic arrangement in a polyhedral chain is illustrated in Figure 4. The Cu^{2+} cations are clearly displaced toward one of the rectangular faces of the trigonal prism in an ordered manner.

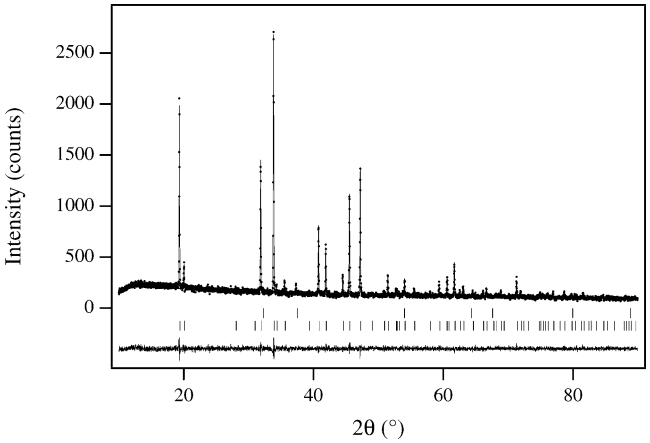

Figure 2. Observed (■), calculated (—), and difference X-ray powder diffraction patterns of $Ca_{3.1}Cu_{0.9}MnO_6$ at 302 K. Reflection positions for the main phase (lower) and CaO (upper) are marked.

Table 1. Structural Parameters of Rhombohedral $Ca_{3.1}Cu_{0.9}MnO_6$ at 302 K[a]

a/Å		9.1511(2)
c/Å		10.6327(2)
Ca	*x*	0.3632(4)
Ca	U_{iso}/Å^2	0.030(2)
Cu/Ca[b]	*x*	−0.044(1)
Cu/Ca[b]	U_{iso}/Å^2	0.034(4)
Mn	U_{iso}/Å^2	0.026(2)
O	*x*	0.1755(7)
O	*y*	0.0243(9)
O	*z*	0.1059(5)
O	U_{iso}/Å^2	0.026(2)
R_{wp}/%		8.50
χ^2		1.119

[a] Space group: $R\bar{3}c$. Ca: (18*e*) *x*, 0, $^1/_4$. Mn: (6*b*) 0, 0, 0. Cu/Ca: (18*e*) *x*, 0, $^1/_4$. O: (36*f*) *x*, *y*, *z*. [b] Total site occupancy = $^1/_3$.

(14) Moore, C. A. D. Phil. Thesis, University of Oxford, 2003.

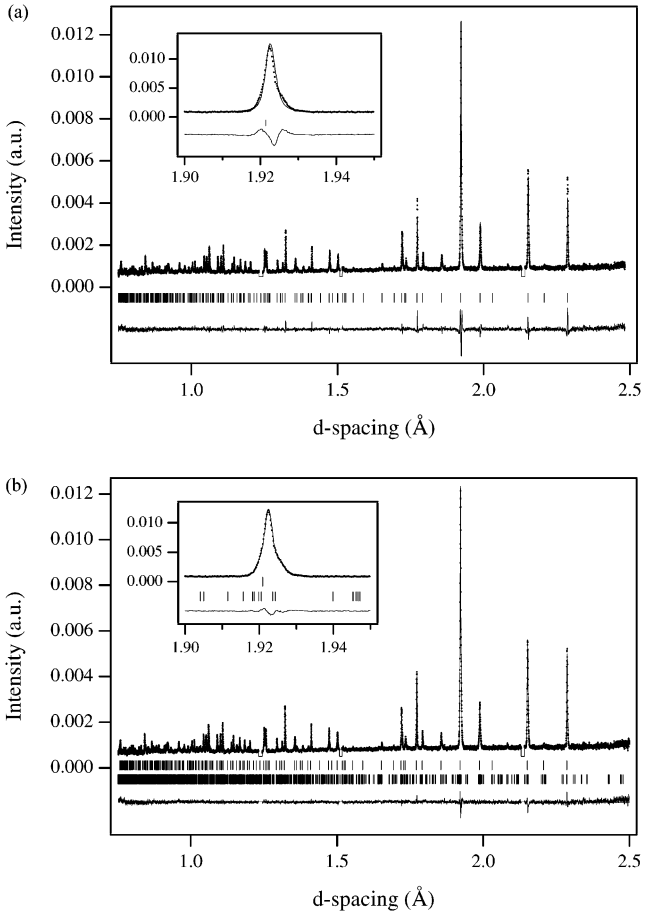

Figure 3. Observed (■), calculated (—), and difference neutron powder diffraction patterns of $Ca_{3.1}Cu_{0.9}MnO_6$ collected on HRPD at 293 K and modeled (a) using a rhombohedral structure and (b) as a two-phase mixture; reflection positions for the rhombohedral (upper) and triclinic (lower) phases are marked. The inset shows the intense 223 peak with an obvious shoulder.

In view of the results of the neutron diffraction experiments described above, further X-ray diffraction data were collected as a function of temperature between 300 and 16 K. A data set collected at 300 K could be analyzed using a rhomobohedral model, but a triclinic phase was also apparent at 294 K, and the latter was dominant at 288 K. Two-phase structural refinements based on X-ray data lead us to conclude that the phase transition occurs at 290 ± 3.5 K, which is consistent with the observation of two phases in neutron data collected at 293 K. X-ray data collected at 16 K could be interpreted as arising solely from a triclinic phase.

(ii) $Sr_3Cu_{1-x}M_xIrO_6$ (M = Ni, Zn; $0 \le x \le 0.5$). The X-ray diffraction patterns collected at room temperature on samples in this series having M = Zn were consistent with the results published previously by Niazi et al. Compositions having $x \le 0.4$ were monoclinic, whereas the sample having $x = 0.5$ was rhombohedral. The same composition dependence was observed in samples having M = Ni. The X-ray diffraction pattern of samples with $x \le 0.4$, for both M = Ni and M = Zn, was found to change on heating (Figure 6a) in a way that was consistent with a transition from monoclinic to rhombohedral symmetry. The composition dependence of the estimated transition temperatures is plotted in Figure 6b.

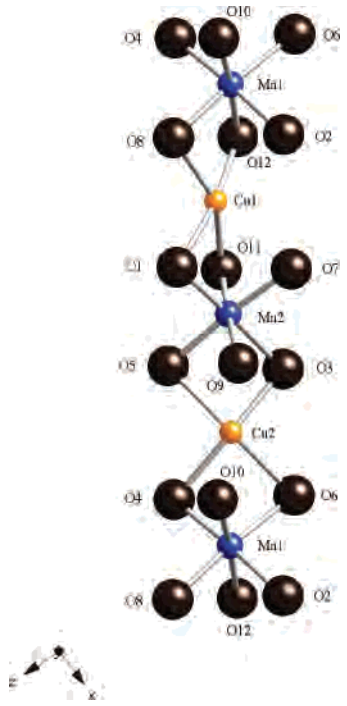

Figure 4. Details of the polyhedral chains within triclinic $Ca_{3.1}Cu_{0.9}MnO_6$.

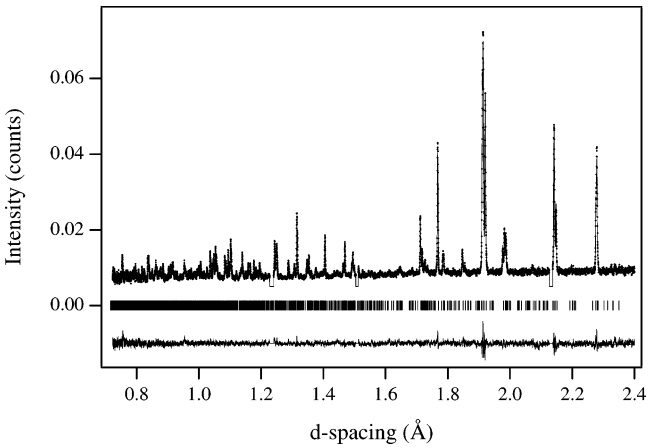

Figure 5. Observed (■), calculated (—), and difference neutron powder diffraction patterns of $Ca_{3.1}Cu_{0.9}MnO_6$ at 2 K collected on HRPD and modeled as a triclinic structure.

Table 2. Lattice Parameters of Triclinic $Ca_{3.1}Cu_{0.9}MnO_6$ Derived from Neutron Diffraction Data

	293 K	2 K
a/Å	8.8241(3)	8.810(1)
b/Å	9.1477(3)	9.1310(1)
c/Å	6.3645(2)	6.35653(9)
α/deg	90.120(2)	90.240(1)
β/deg	92.799(2)	92.675(1)
γ/deg	90.104(2)	90.183(1)

(iii) $Ca_{3.1}Cu_{0.9}RuO_6$. The X-ray and neutron diffraction patterns recorded from the reaction product at 302 K could both be fitted in a satisfactory manner (R_{wp} = 6.1% for neutron diffraction) using the monoclinic structural model described previously for this composition.[13] DSC data showed evidence of a phase transition at 630 K, and neutron diffraction patterns were therefore recorded at 20 K intervals between 523 and 723 K in order to span the transition. The evolution of the diffraction pattern with temperature is shown

Table 3. Structural Parameters of Triclinic ($P\bar{1}$) $Ca_{3.1}Cu_{0.9}MnO_6$ at 293 and 2 K by Neutron Diffraction

		293 K	2 K			293 K	2 K
Ca1	*x*	0.003(4)	0.009(2)	O2	*x*	0.066(3)	0.065(1)
	y	0.390(3)	0.395(1)		*y*	0.162(3)	0.157(1)
	z	0.252(5)	0.242(2)		*z*	0.048(4)	0.051(2)
Ca2	*x*	0.496(4)	0.491(1)	O3	*x*	0.445(3)	0.441(1)
	y	0.897(3)	0.890(1)		*y*	0.658(3)	0.652(1)
	z	0.245(5)	0.232(2)		*z*	0.461(4)	0.462(2)
Ca3	*x*	0.681(4)	0.686(2)	O4	*x*	0.559(3)	0.567(1)
	y	0.569(3)	0.571(1)		*y*	0.657(3)	0.651(1)
	z	0.380(5)	0.371(2)		*z*	0.053(4)	0.060(2)
Ca4	*x*	0.336(3)	0.319(2)	O5	*x*	0.276(3)	0.268(1)
	y	0.562(3)	0.564(1)		*y*	0.678(2)	0.686(1)
	z	0.115(4)	0.118(2)		*z*	0.796(4)	0.788(2)
Ca5	*x*	0.196(3)	0.188(2)	O6	*x*	0.726(3)	0.732(1)
	y	0.081(3)	0.079(1)		*y*	0.672(3)	0.682(1)
	z	0.375(4)	0.386(2)		*z*	0.716(4)	0.704(2)
Ca6	*x*	0.797(3)	0.823(1)	O7	*x*	0.760(3)	0.762(1)
	y	0.065(3)	0.067(1)		*y*	0.182(3)	0.178(1)
	z	0.097(4)	0.115(2)		*z*	0.784(4)	0.782(2)
Mn1	*x*	0.248(4)	0.252(2)	O8	*x*	0.247(3)	0.217(1)
	y	0.245(4)	0.247(2)		*y*	0.192(3)	0.187(1)
	z	0.001(7)	0.004(3)		*z*	0.713(4)	0.724(2)
Mn2	*x*	0.763(4)	0.757(2)	O9	*x*	0.364(3)	0.366(1)
	y	0.270(3)	0.252(2)		*y*	0.927(2)	0.927(1)
	z	0.512(6)	0.501(3)		*z*	0.566(4)	0.573(1)
Cu1[a]	*x*	−0.013(2)	−0.019(1)	O10	*x*	0.628(3)	0.632(1)
	y	0.739(2)	0.7268(8)		*y*	0.913(2)	0.923(1)
	z	0.278(3)	0.292(1)		*z*	0.928(4)	0.927(2)
Cu2[a]	*x*	0.499(2)	0.496(1)	O11	*x*	0.860(3)	0.865(1)
	y	0.307(2)	0.3029(8)		*y*	0.421(3)	0.422(1)
	z	0.245(3)	0.252(1)		*z*	0.580(3)	0.572(2)
O1	*x*	0.936(3)	0.931(1)	O12	*x*	0.134(3)	0.129(1)
	y	0.154(3)	0.160(1)		*y*	0.413(3)	0.412(1)
	z	0.456(4)	0.455(2)		*z*	0.925(4)	0.908(2)
R_{wp}/%	4.19	4.63					
χ^2	2.700	1.847					

[a] 90% Cu, 10% Ca.

Table 4. Selected Bond Lengths (Å) of $Ca_{3.1}Cu_{0.9}MnO_6$ Derived from Neutron Powder Diffraction Data

	$R\bar{3}c$ 293 K		$P\bar{1}$ 293 K	$P\bar{1}$ 2 K
Cu−O	2.006(3) ×2	Cu1−O1	2.05(3)	2.03(2)
	2.076(2) ×2	Cu1−O2	2.29(3)	2.44(1)
	2.496(5) ×2	Cu1−O7	2.40(3)	2.49(1)
		Cu1−O8	2.16(3)	1.91(2)
		Cu1−O11	2.16(3)	2.08(2)
		Cu1−O12	2.14(3)	2.00(2)
		Cu2−O3	1.94(3)	1.92(2)
		Cu2−O4	1.97(3)	2.08(2)
		Cu2−O5	2.02(3)	2.11(2)
		Cu2−O6	2.02(4)	2.04(2)
		Cu2−O9	2.72(3)	2.65(1)
		Cu2−O10	2.52(3)	2.58(1)
mean short Cu−O	2.041(3)		2.06(3)	2.02(2)
mean long Cu−O	2.496(5)		2.48(3)	2.54(1)
Mn−O	1.905(3) ×6	Mn1−O2	1.81(4)	1.87(2)
		Mn1−O4	1.97(4)	1.91(2)
		Mn1−O6	1.95(5)	1.96(2)
		Mn1−O8	1.89(5)	1.87(2)
		Mn1−O10	1.86(4)	1.90(2)
		Mn1−O12	1.88(4)	1.94(2)
		Mn2−O1	1.91(5)	1.79(2)
		Mn2−O3	1.97(4)	1.97(2)
		Mn2−O5	2.03(4)	1.93(2)
		Mn2−O7	1.91(4)	1.91(2)
		Mn2−O9	2.16(4)	2.00(2)
		Mn2−O11	1.67(4)	1.86(2)
mean Mn−O	1.905(3)		1.92(4)	1.91(2)

in Figure 7. The data collected in the range $623 \leq T/K \leq 723$ could all be indexed using a rhombohedral unit cell in space group $R\bar{3}c$, and the intensity distribution was accounted for by a structural model based on the Sr_4PtO_6 structure with Ca1 cations occupying the interchain (18*e*) cation sites and Ca2 occupying 10% of the prismatic sites. However, a difference Fourier map showed clear evidence of a disordered displacement of some cations on the prismatic sites toward the rectangular faces of the prism. The final analyses of these data sets were therefore carried out with only the minority Ca2 cations located at the 6*a* site on the 3-fold axis, and with the Cu^{2+} cations occupying off-axis 18*e* sites with a fractional occupancy of 0.3. Anisotropic displacement parameters were applied to all atoms other than Cu1 and Ca2 in the prismatic site, which were constrained to have the same isotropic displacement parameter. This disordered model gave a good fit to the data throughout the high temperature region, as exemplified by Figure 8a. A full listing of the structural and displacement parameters derived for the rhombohedral phase from the neutron diffraction data sets is presented in Tables S1 and S2, and the bond lengths are listed in Table S3; the disorder in the prismatic site at 623 K is represented in Figure 9. Each of the three partially occupied Cu sites lies 0.524(3) Å from the centroid of the prism, and the intersite distance is 0.908(3) Å.

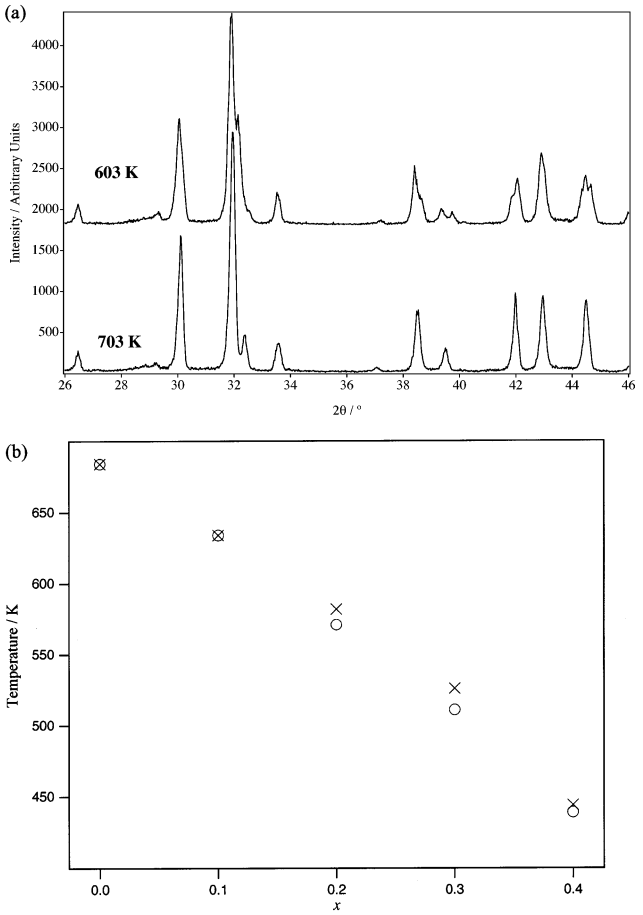

Figure 6. (a) X-ray powder diffraction pattern of $Sr_3Cu_{0.9}Zn_{0.1}IrO_6$ as a function of temperature and (b) composition dependence of the monoclinic−rhombohedral phase transition temperature in $Sr_3Cu_{1-x}M_xIrO_6$ (M = Ni (X), Zn (O)).

A monoclinic unit cell in space group *C*2/*c* was required in order to index and analyze the data collected at 603 K

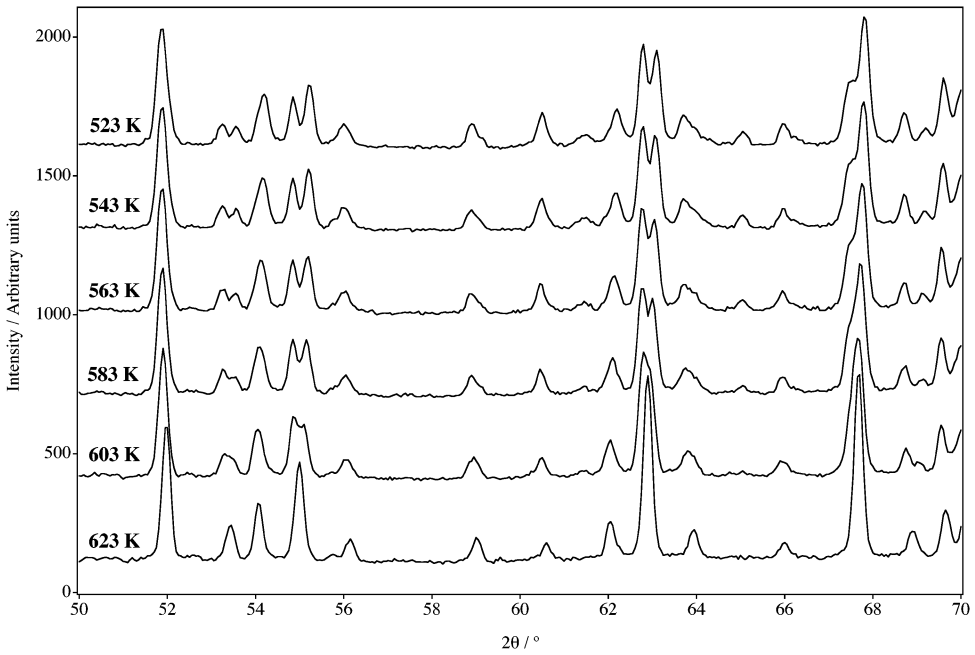

Figure 7. Neutron powder diffraction pattern of $Ca_{3.1}Cu_{0.9}RuO_6$ as a function of temperature.

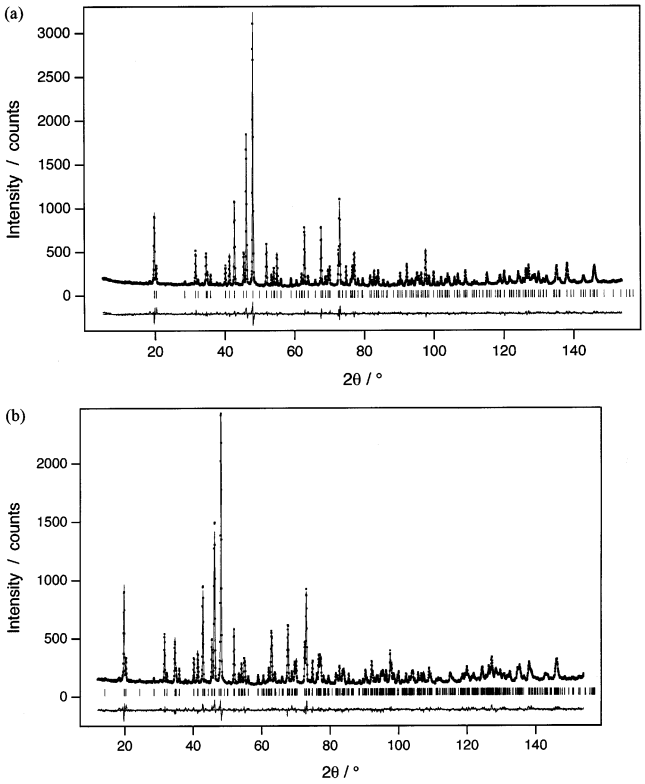

Figure 8. Observed (■), calculated (—), and difference neutron powder diffraction patterns of $Ca_{3.1}Cu_{0.9}RuO_6$ at (a) 623 K, modeled as a rhombohedral structure, and (b) at 603 K, modeled as a monoclinic structure.

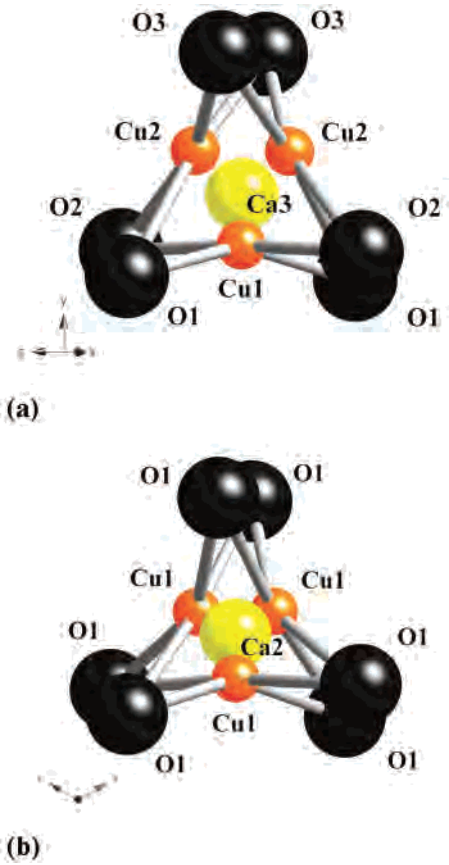

Figure 9. Detail of the prismatic site of $Ca_{3.1}Cu_{0.9}RuO_6$ in (a) the low temperature monoclinic phase and (b) the high temperature rhombohedral phase.

and lower temperatures. However, the fully ordered model previously used to describe the Cu-containing members of this structural family proved to be inadequate for this system. Rather than modeling the prismatic site with a single cation (Cu1) on a 4*e* site located (Figure 1) close to a rectangular face of the prism and lying on the 2-fold axis that passes through the polyhedron, it was necessary to include a second site (Cu2) on an 8*f* position off the 2-fold axis (Figure 9), thus generating Cu atoms close to the other two rectangular faces. The prismatically coordinated Ca3 cations were located on 4*e* sites close to the centroid of the prism; Ca1 and Ca2 occupy the cation sites between the polyhedral chains. A typical fit to a neutron diffraction pattern is shown in Figure

Table 5. Structural Parameters and Bond Lengths (Å) for $Ca_{3.1}Cu_{0.9}RuO_6$ at 603 and 623 K[a]

temperature 603 K			temperature 623 K		
space group	*C*2/*c*		space group	$R\bar{3}c$	
V/Å^3 ($Z = 4$)	544.35(3)		V/Å^3 ($Z = 6$)	816.98(3)	
a/Å	9.0269(2)		a/Å	9.2903(1)	
b/Å	9.2957(2)		c/Å	10.9299(2)	
c/Å	6.4911(2)				
β/deg	91.982(1)				
R_{wp}/%	4.97		R_{wp}/%	5.06	

temperature 603 K					temperature 623 K				
Ca1	x	0.8961(7)	Ca1−O1 ×2	2.705(7)	Ca1	x	0.3593(2)	Ca1−O1 ×2	2.350(2)
	U_{iso}/Å^2	0.023(1)	Ca1−O2 ×2	2.596(3)		U_{eq}/Å^2	0.0206(9)	Ca1−O1 ×2	2.521(1)
Ca2	x	0.6804(4)	Ca1−O3 ×2	2.484(3)	Cu1	x	−0.0564(3)	Ca1−O1 ×2	2.679(2)
	y	0.5716(5)	Ca1−O3 ×2	2.358(5)		U_{iso}/Å^2	0.028(1)	Ca1−O1 ×2	2.515(1)
	z	0.3879(6)	Ca2−O1	2.337(5)		f	0.3		
	U_{iso}/Å^2	0.0166(6)	Ca2−O1	2.522(5)	Ru1	U_{eq}/Å^2	0.014(8)		
Cu1	y	0.6951(9)	Ca2−O1	2.561(6)	O1	x	0.1822(2)		
	U_{iso}/Å^2	0.026(1)	Ca2−O2	2.340(5)		y	0.0237(1)		
	f[b]	0.583(11)	Ca2−O2	2.688(6)		z	0.10813(9)		
Ca3	y	0.750(2)	Ca2−O2	2.510(6)		U_{eq}/Å^2	0.0265(6)		
	U_{iso}/Å^2	0.026(1)	Ca2−O3	2.430(5)	Ca2	U_{iso}/Å^2	0.028(1)		
	f	0.1				f	0.1		
Cu2	x	0.470(2)	Ca2−O3	2.670(5)					
	y	0.786(2)	Ru−O1 ×2	1.989(3)				Ru1−O1 ×6	1.9840(9)
	z	0.809(3)	Ru−O2 ×2	2.006(4)					
	U_{iso}/Å^2	0.026(1)	Ru−O3 ×2	1.959(3)					
	f	0.159(6)	Cu1−O1 ×2	2.045(4)				Cu1−O1 ×2	2.054(1)
Ru1	U_{iso}/Å^2	0.0122(5)	Cu1−O2 ×2	2.065(3)				Cu1−O1 ×2	2.136(1)
O1	x	0.9398(3)	Cu1−O3 ×2	2.697(8)				Cu1−O1 ×2	2.623(3)
	y	0.1490(4)	Cu2−O1	2.15(2)					
	z	0.4506(5)	Cu2−O1	2.66(2)					
	U_{iso}/Å^2	0.0188(7)	Cu2−O2	2.00(2)					
O2	x	0.248(3)	Cu2−O2	2.60(2)					
	y	0.6840(4)	Cu2−O3	2.19(2)					
	z	0.7934(5)	Cu2−O3	2.10(2)					
	U_{iso}/Å^2	0.0254(8)	Ca3−O1 ×2	2.207(9)				Ca2−O1 ×6	2.224(1)
O3	x	0.3629(3)	Ca3−O2 ×2	2.150(7)					
	y	0.9238(4)	Ca3−O3 ×2	2.32(1)					
	z	0.5729(5)							
	U_{iso}/Å^2	0.0214(7)							

[a] 603 K model (*C*2/*c*), Ca1: (4*e*) $^1/_2$, *y*, $^1/_4$. Ca2: (8*f*) *x*, *y*, *z*. Ru: (4*c*) $^3/_4$, $^3/_4$, 0. Cu1: (4*e*) $^1/_2$, *y*, $^3/_4$. Ca3: (4*e*) $^1/_2$, *y*, $^3/_4$. Cu2: (8*f*) *x*, *y*, *z*. O1, O2, O3: (8*f*) *x*, *y*, *z*. 623 K model ($R\bar{3}$c), Ca1: (18*e*) *x*, 0, $^1/_4$. Ru1: (6*b*) 0, 0, 0. Cu1: (18*e*) *x*, 0, $^1/_4$. Ca2: (6*a*) 0, 0, $^1/_4$. O1: (36*f*) *x*, *y*, *z*. [b] The fractional occupancy of a site on a disordered sublattice.

8b, and full listings of the structural parameters and bond lengths as a function of temperature in the monoclinic phase are given in Tables S4 and S5, respectively. Isotropic displacement factors were used in modeling the monoclinic phase, with all the prismatic sites constrained to take the same value. As illustrated in Figure 9, there are three Cu sites (Cu1 + 2Cu2) in each prism, and the monoclinic symmetry is consistent with their having unequal fractional occupation factors. The phase transition which occurs in the range $603 \leq T/\mathrm{K} \leq 623$ thus involves passing from a disordered, rhombohedral high temperature phase in which the three Cu^{2+} sites within a prism have equal occupation factors to a disordered, monoclinic, low temperature phase in which one of the four-coordinate sites (Cu1) is preferred to the other two. Figure 10 shows the temperature dependence of the ordering parameter, defined as

$$\left(m_1 f_1 - \frac{1}{n-1}\sum_{2}^{n} m_i f_i\right) \Big/ \sum_{1}^{n} m_i f_i$$

where site 1 is the preferred site, m_i and f_i are the multiplicity and fractional occupancy of the ith site and $n = 3$ in the present case; the structure becomes more ordered on cooling as the imbalance between the occupation factors increases. The steady growth of the 243 Bragg reflection at $2\theta = 65°$ (Figure 7) is the clearest observable indicator of this behavior. The structural parameters and bond lengths determined from data collected at the two temperatures, 603 and 623 K, which straddle the phase transition are summarized in Table 5.

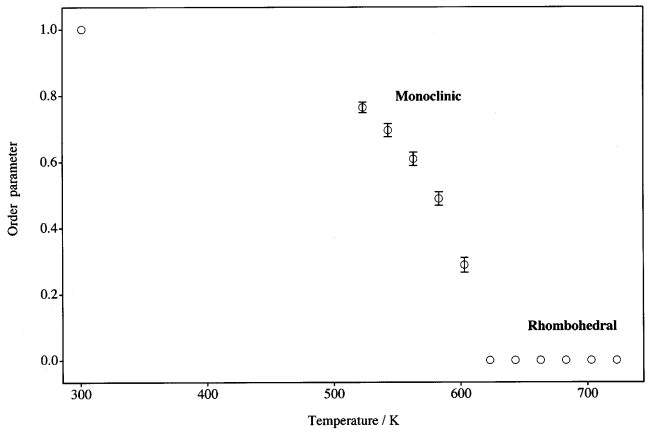

Figure 10. Temperature dependence of the order parameter of monoclinic $Ca_{3.1}Cu_{0.9}RuO_6$.

Discussion

The bonding and coordination requirements of the cations Ni^{2+} and Zn^{2+} in an oxide environment often differ considerably, despite the similarity of their ionic radii. The observation (Figure 6) that the composition dependence of the temperature at which the structural phase transition occurs in $Sr_3Cu_{1-x}M_xIrO_6$ is essentially the same for M = Ni and Zn therefore suggests that the structural chemistry of these systems is primarily determined by the bonding requirements of the Cu^{2+} cations, and the remainder of this discussion will focus on the environment of this species.

In view of the relatively high Cu-concentration, it was surprising to observe rhombohedral symmetry in the first X-ray diffraction patterns of $Ca_{3.1}Cu_{0.9}MnO_6$, particularly in the light of the report by Zubkov et al. in which a triclinic structure was assigned to a compound with a very similar composition. Furthermore, no rhombohedral Cu-rich $A_3A'BO_6$ phase has been reported previously, although a single crystal of $Sr_3(Ru_{0.336}Pt_{0.664})CuO_6$ was thought[15] to be rhombohedral until the presence of twinning was recognized; twinning is unlikely to be a problem in a powder diffraction experiment. Our subsequent studies showed that a rhombohedral/triclinic phase transition occurs in $Ca_{3.1}Cu_{0.9}MnO_6$ at a temperature so close to ambient that a difference in the meaning of ambient in two different laboratories could be crucial in a comparison of results. However, Zubkov et al. kindly made their sample available to us, and we were able to demonstrate that it is not rhombohedral at 302 K; the small difference in composition between the two samples clearly has a significant effect on the structural chemistry.

In the triclinic form of $Ca_{3.1}Cu_{0.9}MnO_6$, the Jahn−Teller induced displacements of the Cu^{2+} cations show long-range order throughout the crystal structure, whereas in the rhombohedral form there are only local, disordered displacements off the 3-fold axis. The low transition temperature of $Ca_{3.1}Cu_{0.9}MnO_6$ must reflect a relatively low energy difference between the two forms. The gain in bond energy on ordering is presumably relatively small compared to the elastic energy associated with the transition. It is not clear why this compound behaves differently from the other phases studied to date, which all adopt a monoclinic structure at low temperatures. The most useful contrast is with $Ca_{3.1}Cu_{0.9}RuO_6$; the only obvious difference between these two compounds is the size of the cation on the octahedral site, a Ru^{4+}−O bond being longer than a Mn^{4+}−O bond by ∼0.07 Å. The low symmetry leads to relatively low precision in the structural parameters and bond lengths (Tables 3 and 4), particularly at 293 K, but it is apparent that the mean lengths of the four shortest bonds around Cu2 (2.04 Å) and Cu1 (2.01 Å) are similar to each other and to those observed in related compounds.[9,13,16] The two prismatic sites differ in that the two long bonds around Cu2 are significantly longer than the corresponding bonds around Cu1. There are relatively few examples of Cu^{2+} in trigonal prismatic coordination outside this structural family. However, the mineral claringbullite[17] contains a Cu sublattice very similar to that described above for the rhombohedral form of $Ca_{3.1}Cu_{0.9}MnO_6$. In the mineral, the Cu cations are displaced in a disordered manner off a 3-fold axis toward one of the rectangular faces of a prism. The four short Cu−O distances are 1.988(2) Å, and the longer distances are 2.438(3) Å, making the prism slightly smaller than that in $Ca_{3.1}Cu_{0.9}MnO_6$. The two Mn-containing octahedra in $Ca_{3.1}Cu_{0.9}MnO_6$ have the same average Mn−O bond length (1.91 Å) which is close to that (1.90 Å) observed in $BaMnO_3$ at 1.7 K.[18] The bond lengths in our sample are similar to those listed by Zubkov et al., although they report a larger difference between the two prismatic sites.

The results discussed above demonstrate that the presence of Cu in $A_3A'BO_6$ compounds can induce phase transitions over a wide temperature range and to more than one low temperature form. Our study of $Ca_{3.1}Cu_{0.9}RuO_6$ was intended to reveal the details of the structural changes that occur immediately above and below the transition temperature. On cooling through the phase transition the environment of the Ru cation changes very little, and the single Ca interchain site simply splits into a relatively large site (mean Ca1−O = 2.536(5) Å) and a smaller site (mean Ca2−O = 2.507(5) Å) which then show no significant change on cooling to 302 K. However, the bond lengths around the Cu1 site (Table S4) do change as the population of the site increases; the mean of the four short distances to oxide ions (O1 and O2) in the nearby rectangular face of the prism decreases from 2.055(4) to 2.016(3) Å whereas the distance to the other two oxide ions (O3) increases from 2.697(8) to 2.784(3) Å. Interestingly, the Ca3 cation which occupies 10% of the prismatic sites appears to move closer to O3 and away from O1 and O2 as the fully ordered monoclinic structure develops. The triangle formed by the three partially occupied Cu sites within a prism expands on cooling, with the Cu1 and Cu2 sites distant 0.537(8) and 0.57(2) Å, respectively, from the centroid at 603 K, increasing to 0.569(4) and 0.73(3) Å on cooling to 523 K. The distance between the favored and unfavored sites, Cu1−Cu2, is 0.908(3) Å at 603 K, increasing to 1.19(2) Å at 523 K. These changes lengthen the pathway along which the Cu^{2+} cations must migrate in order to achieve complete ordering.

In the light of these data, the phase change can be regarded as an order/disorder transition, with the entropically-favored, local 3-fold disordered displacements of the Cu^{2+} cations, induced in the high-temperature rhombohedral phase by the Jahn−Telleractivity of the d^9 species, ordering in a periodic manner throughout the structure with a concomitant reduction in symmetry to monoclinic. Figure 10 shows that the ordering is incomplete 100 K below the onset temperature, but that it is complete by 300 K. We therefore regard this as a second-order phase transition. The dynamics of the transition could form the basis of a future study. It would also be interesting to collect neutron diffraction data as function of

(15) Friese, K.; Kienle, L.; Duppel, V.; Luo, H.; Lin, C. *Acta Crystallogr., Sect. B* **2003**, *59*, 182−189.
(16) Tomaszewska, A.; Muller-Buschbaum, H. *Z. Anorg. Allg. Chem.* **1993**, *619*, 534−536.
(17) Burns, P. C.; Cooper, M. A.; Hawthorne, F. C. *Can. Mineral.* **1995**, *33*, 633−639.
(18) Cussen, E. J.; Battle, P. D. *Chem. Mater.* **2000**, *12*, 831−838.

temperature on $Ca_{3.1}Cu_{0.9}MnO_6$ in order to determine if the transition from the rhombohedral to the triclinic phase proceeds in a similar manner.

Conclusions

We have demonstrated that the presence of a high Cu concentration in $A_3A'BO_6$ phases can cause structural phase transitions in the temperature range $290 \leq T/K \leq 700$. In the case of $Ca_{3.1}Cu_{0.9}RuO_6$, the transition is of an order−disorder type and takes place over a temperature range >100 K.

Acknowledgment. We are grateful to EPSRC for financial support (GR/R01194 and GR/R88601) and to R. M. Ibberson and E. Suard for experimental assistance at ISIS and ILL, respectively.

Supporting Information Available: Table S1 listing structural parameters of rhombohedral $Ca_{3.1}Cu_{0.9}RuO_6$ as a function of temperature. Table S2 listing atomic displacement parameters of rhombohedral $Ca_{3.1}Cu_{0.9}RuO_6$ as a function of temperature. Table S3 listing bond lengths in rhombohedral $Ca_{3.1}Cu_{0.9}RuO_6$ as a function of temperature. Table S4 listing structural parameters of monoclinic $Ca_{3.1}Cu_{0.9}RuO_6$ as a function of temperature. Table S5 listing bond lengths in monoclinic $Ca_{3.1}Cu_{0.9}RuO_6$ as a function of temperature. This material is available free of charge via the Internet at http://pubs.acs.org.

IC0487629